Critical backwash flux for high backwash efficiency: Case of ultrafiltration of bentonite suspensions

Thomas Vroman, François Beaume, Valentine Armanges, Emilie Gout, Jean-Christophe Remigy

Critical backwash flux for high backwash efficiency: Case of ultrafiltration of bentonite suspensions

Thomas Vroman[1], François Beaume[2], Valentine Armanges[1], Emilie Gout[1], Jean-Christophe Remigy[1]*

[1] Laboratoire de Génie Chimique, Université de Toulouse, CNRS, INPT, UPS, Toulouse, France (vroman@chimie.ups-tlse.fr, remigy@chimie.ups-tlse.fr)
[2] Arkema, Pierre-Bénite, France (francois.beaume@arkema.com)
** Corresponding author*

ABSTRACT

Optimization of the backwash operating conditions for a specific membrane-feed system can become an initial step to reduce energy and ultrafiltrated water consumption. In this work, fouling removal mechanisms of bentonite cakes were investigated on ultrafiltration Kynar® polyvinylidene fluoride (PVDF) hollow fibre membranes having different dimensions, mechanical and surface properties and water permeability. The study on different bentonite cake structures, formed in dead-end filtration at constant pressure and in outside-in mode, has demonstrated that cake removal mechanism was mainly governed by the backwash flux and not by the intrinsic membrane properties. We define a critical backwash flux, from which backwash becomes efficient. The critical backwash is related to a critical inter cake-membrane pressure which occurs at the cake-membrane interface during backwash, which really acts on the deposit. A fouling removal mechanism is thus proposed involving three steps related the critical inter cake-membrane pressure. The critical inter cake-membrane pressure required for an efficient backwash was independent of the membrane properties and bentonite hydraulic resistance. The critical backwash flux can be used to optimize the energy efficiency of the ultrafiltration process.

KEYWORDS

Ultrafiltration membrane; membrane properties; fouling removal; backwash efficiency; critical backwash flux;

NOMENCLATURE

D_{ext}	hollow fibre membrane external diameter (µm)
h	hollow fibre membrane thickness (µm)
E	membrane Young's Modulus (MPa)
σ_{break}	stress at break (MPa)
ε_{break}	elongation at break (%)
$\varepsilon_{elastic\ limit}$	elongation at elastic limit (%)
WCA	water contact angle (°)
Lp_{TMP}	outside-in membrane permeability at specific TMP (L m^{-2} h^{-1} bar^{-1})
Lp'_{BTMP}	inside-out membrane permeability at specific BTMP (L m^{-2} h^{-1} bar^{-1})
Lp'_{f}	inside-out fouled membrane permeability (L m^{-2} h^{-1} bar^{-1})
V_p	permeate volume (L)
T	temperature (°C)
V_{bw}	backwash volume (L)
S_{ext}	hollow fibre membrane external surface (m^2)
TMP	transmembrane pressure (bar)
$BTMP$	backwash transmembrane pressure (bar)
$BTMP_{crit}$	critical backwash transmembrane pressure (bar)
$ICMP$	inter cake-membrane pressure (bar)
$ICMP_{crit}$	critical inter cake-membrane pressure (bar)
J	permeate flux (L m^{-2} h^{-1})
J_{bw}	backwash flux through the fouled membrane (L m^{-2} h^{-1})
$J_{bw,crit}$	critical backwash flux (L m^{-2} h^{-1})
μ_s	solvent viscosity (bar h)
t	time (h)
R_m	outside-in membrane hydraulic resistance at specific TMP (m^2 L^{-1})
R'_m	inside-out membrane hydraulic resistance at specific BTMP (m^2 L^{-1})
R_c	cake hydraulic resistance (m^{-1} or m^2 L^{-1})

m_d	deposited mass on membrane external surface (kg)
m_{bw}	mass of bentonite cake collected in the backwash waters (kg)
CR	amount of cake removed during the backwash
e_f	energy consumption for a single filtration (J)
e_{bw}	energy consumption for a single backwash (J)

1. Introduction

Membrane ultrafiltration is increasingly used for water treatment to remove suspended matter, colloidal particles, bacteria or viruses [1] from a wide range of water quality (i.e. domestic or industrial effluents, natural surface water). Even if membrane filtration is experiencing a strong industrial development, fouling remains one of the major limitation in water filtration. Fouling of membranes during filtration results in a drop in productivity and membranes need to be regularly cleaned to recover their initial permeability. Backwash is a physical cleaning process commonly used in water filtration to eliminate the reversible deposit from the hollow fibre membrane surface [2] . However after several filtration and backwash cycles a decrease of permeability is observed on the long term, this decrease is often attributed to irreversible fouling mechanisms such as adsorption [3], [4] or biofilm formation [5]. It could yet be assumed that the reversible deposit was not completely removed during the backwash step and would therefore lead to a quicker and stronger build-up of the new cake layer for the next cycles [6]. Remize *et al.* [7] have highlighted the existence of a remaining fouling after the backwash and demonstrated that improving the backwash efficiency could reduce the long term decrease in permeability. A high backwash efficiency with minimum residual deposit would limit the need of chemical cleanings which are involved in membrane ageing [8], [9], [10].

Extensive works have been published on fouling, fouling mitigation and fouling removal [11], [12], [13], [14], [15]. In particular, the pioneer works of Bacchin and Aimar show experimentally and theoretically, the role of electrostatic interactions in colloidal fouling during the filtration [16], [17]. The Bacchin and Aimar works also emphases the role of the local flux distribution over the membrane surface due to the pore size distribution and the heterogeneity of the selective layer (i.e. pore size distribution, skin thickness,

…). They defined, and measured, a critical flux during filtration above which an irreversible fouling occurs through the aggregation of colloids at the membrane surface and the formation of a colloidal gel (i.e. the cake). Thus, the critical flux depends on the operating conditions but also on the ionic strength linked to the charge and concentration of ions. Aggregation of colloidal particles leads to the formation of a cake whose mechanical and hydraulic properties or their structure depend on the nature and concentration of salts present in the suspension [18], [19], [20], [21]. Thus, cakes with different mechanical and hydraulic properties could be formed from the same nanoparticle suspension (i.e. bentonite particles in this study) but with different salts at the same ionic strength.

However, fouling removal mechanisms are still poorly understood and literature focusing on backwash optimization is limited [2]. Many technological aids have been implemented in industries to improve the backwash efficiency such as air sparging which is commonly used in membrane bioreactors [22], [23], [24]. Indeed the injection of air bubbles in parallel with backwashing introduces shear stress at membrane surface which greatly helps for fouling removal [25][26]. Furthermore, backwash operating conditions and in particular backwash frequency, backwash duration and relaxation time can been optimized to control fouling and reduce the long term decrease in permeability [2], [27], [28], [29]. A few works have shown the influence of the applied backwash pressure [7] or the backwash flux [30], [31] on the fouling removal but optimal conditions were not described. Huang *et al.* [30] demonstrated that reversible fouling removal could be improved by increasing the backwash flux and that hydrodynamic conditions were unique to the membrane material and type of foulants. A recent work from the M. Wessling team [32] described the microscopic events that occur during backwashing using microfluidic chips (20 µm pore size) and polystyrene particles (4.2 µm). From experimental study, the authors described three phenomena that occurs when increasing the backwash velocity: Detachment of cluster of particles (i.e. aggregates), fragmentation of cluster and partial removal of particle aggregates from the pore structure. From a multiphase simulation study on the backwash of a cake over one pore, they show the backwash efficiency should suddenly increase with pore fluid velocity

depending on the particle to membrane interaction and the particle to particle interaction. Finally, the particle to membrane interaction dominantly controls the backwash efficiency.

Regarding the influence of the membrane surface properties on the fouling removal, Chang *et al.* [33] observed a higher backwash efficiency on fouled hydrophilic membrane rather than on fouled hydrophobic membrane due to difference in surface free energy of adhesion between foulant and membrane. It is also suggested that mechanical properties can affect the backwash efficiency. Indeed, Akhondi *et al.* [34] have shown an enlargement of the pores of PVDF hollow fibre membranes when applying the backwash pressure. They also demonstrated that the pore deformation is higher for a membrane with lower Young's Modulus. Levering *et al.* [35] demonstrated that stretching a biofilm-covered silicon flat substrate (without pores) can cause the biofilm detachment. The biofilm debonding was related to the applied strain and strain rate. A minimum of 25% strain and strain rate of 40% per second were however required to detach 80% of the biofilm. By analogy, the membrane surface deformation during the backwash step could lead to a greater fouling removal if the deformation is sufficient.

To the best of our knowledge membrane properties have not been related to optimal backwash conditions in the literature. Due to a lack of knowledge on fouling removal mechanisms, backwash pressures or fluxes are usually chosen by membrane manufacturers or industrials based on the experience [36]. Understanding the fouling removal mechanisms and determining the optimal backwash operating conditions could therefore lead to energy saving and increase production rate of treated water.

Hollow fibre membranes with different dimensions, mechanical and surface properties, and mass transfer properties were selected in this paper to investigate the influence of membrane properties on membrane cleaning and especially on the backwash efficiency. Furthermore, membrane were fouled in dead-end filtration and outside-in mode with bentonite in different saline conditions (KCl or $CaCl_2$) to obtain the different cake properties [37]. Optimal backwash flux conditions (critical backwash flux) were found and correlated with the deposit hydraulic resistance. We defined a needed pressure to detach and remove the bentonite cake whatever the salt used and new insights on the bentonite cake mechanism removal are provided.

2. Experimental

2.1. Materials

Hollow fibre membranes made of various grades of Kynar® polyvinylidene fluoride (PVDF) homo and copolymer from Arkema S.A. (France), with various additives (lithium chloride (LiCl), polyvinylpyrrolidone (PVP) or polyethylene glycol (PEG)): M-LP91, M-HP47, M-HP32 and M-LP19 spun *ad hoc*. Bentonite (montmorillonite) Clarsol FB2 was purchased from CECA (France). Sodium azide (NaN_3) was purchased from Sigma Aldrich (France). Potassium chloride (KCl) was purchased from Carlo Erba (France) and dihydrated calcium chloride ($CaCl_2$, $2H_2O$) from Acros Organics (France).

2.2. Characterization

2.2.1. Hollow fibre membranes

Membrane samples were cryofractured and coated with gold under vacuum before being observed with scanning electron microscopy (SEM, Phenom XL Desktop). Pictures of the cross-sectional area of the membranes were taken to measure the hollow fibre dimensions (outer diameter D_{ext} and thickness h). The global morphology and the inner structure (sponge-like or macroporous structure) were also observed under SEM.

Hollow fibre membranes were mechanically tested using the testing machine (Instron, France) equipped with pneumatic grips for cord and yarn. The initial gauge length was fixed at 85 mm and the elongation rate at 50 mm/min. Specimen was axially elongated up to breaking. Stress-strain curves were processed with BlueHill 2 software (Instron, France). Young's Modulus E, stress at break σ_{break}, elongation at break ε_{break} and elongation at elastic limit $\varepsilon_{elastic\ limit}$ of the membranes were measured in wetted-conditions and ambient temperature. Average data was calculated on 5 samples.

Contact angle from air captive bubble in water was measured on flattened membrane surface at room temperature by a contact angle goniometer (Krüss, Drop Shape Analyzer – DSA30). The injected air bubble volume was 10 µL. Water contact angle for each hollow fibre membrane was averaged over 10 measurements.

Membrane permeability was assessed using a filtration set-up in dead-end filtration and in outside-in and inside-out mode. Membrane was conditioned for 45 minutes at 0.2 bar prior to measure the permeability variations at incremental pressures (from 0.2 to 2.4 bar) with ultrapure water. Membrane permeability was also measured at 0.8 bar before the filtration of bentonite suspensions and after a conditioning step with ultrapure water at 0.8 bar for 45 minutes.

Each membrane permeability was calculated and temperature corrected at 20°C using Eq. 1 and Eq. 2 for the applied pressure in outside-in and inside-out mode as deformable membrane did not show a constant permeability over the pressure range. The external surface was used for both permeability calculations since the filtration was performed in outside-in mode.

$$Lp_{TMP} = \frac{V_p}{S_{ext} * t * TMP} * (1 - 0{,}025 * (20 - T)) \quad \text{Eq. 1}$$

with Lp_{TMP} the membrane permeability (L m^{-2} h^{-1} bar^{-1}), in outside-in mode measured at specific TMP, TMP the transmembrane pressure (bar), V_p the permeate volume (L), S_{ext} the hollow fibre membrane external surface (m²), t the time (h) and T the temperature (°C).

$$Lp'_{BTMP} = \frac{V_p}{S_{ext} * t * BTMP} * \left(1 - 0{,}025 * (20 - T)\right) \quad \text{Eq. 2}$$

with Lp'_{BTMP} the membrane permeability (L m^{-2} h^{-1} bar^{-1}) in inside-out mode measured at specific BTMP, $BTMP$ the backwash transmembrane pressure (bar).

Membrane zeta potential is assumed to be negative at pH 7 as reported in literature for similar membranes made of same polymer and additive [38].

The membrane properties for the Kynar® PVDF hollow fibre membranes are gathered in Table 1.

Table 1: Kynar® PVDF hollow fibre membrane additives and properties: permeability in outside-in mode at TMP=0.8 bar ($Lp_{0.8}$), water contact angle (*WCA*), dimensions (D_{ext}, h) and mechanical properties (E, σ_{break}, ε_{break}, $\varepsilon_{elastic\ limit}$).

Fibre Name	*Addi -tive*	**Permeability**	**Bentonite retention**	**Surface**	**Dimensions**		**Mechanical**			
		$Lp_{0.8}$	%	WCA	D_{ext}	h	E	σ_{break}	ε_{break}	$\varepsilon_{elastic\ limit}$
		L m^{-2} h^{-1} bar^{-1}		°	µm	µm	MPa	MPa	%	%
M-LP91	LiCl	265 ± 20	100	54 ± 3	925 ± 28	180 ± 9	91 ± 5	5.6 ± 0.2	110 ± 6	1.5 ± 0.2
M-HP47	PVP	490 ± 40	100	37 ± 3	1390 ± 42	280 ± 14	47 ± 2	3.7 ± 0.3	104 ± 18	2.6 ± 0.8
M-HP32	PVP	500 ± 30	100	40 ± 2	1350 ± 41	340 ± 17	32 ± 2	2.6 ± 0.1	92 ± 6	2.3 ± 0.4
M-LP19	PEG	150 ± 30	100	50 ± 3	840 ± 25	160 ± 8	19 ± 1	1.6 ± 0.1	140 ± 12	1.8 ± 0.2

Brunauer-Emmett-Teller (BET) analysis was carried out on MicrotracBel nitrogen adsorption analyser, Model Belsorp-max. Dry membranes were cut down, placed into a glass tube and outgassed before analysis. Nitrogen adsorption was measured at 77 K. Pore size distribution was determined from nitrogen adsorption/desorption isotherms using NLDFT model and BET method. As seen on Figure 1, pore size distribution followed a similar pattern for all hollow fibre membranes with higher pore number for membranes with high permeability (M-HP47 and M-HP32) compared to membranes with lower permeability (M-LP91 and M-LP19). It should be noted that during BET analysis both skin and support porosity are taken into account: Large pores are attributed to the support and smaller ones (2 -10 nm) are attributed to the skin layer as pore could not be seen at the membrane surface using SEM (x5000) due to detection limit. Full bentonite retention is observed for all membranes and correlated to the small pore size of the skin layer.

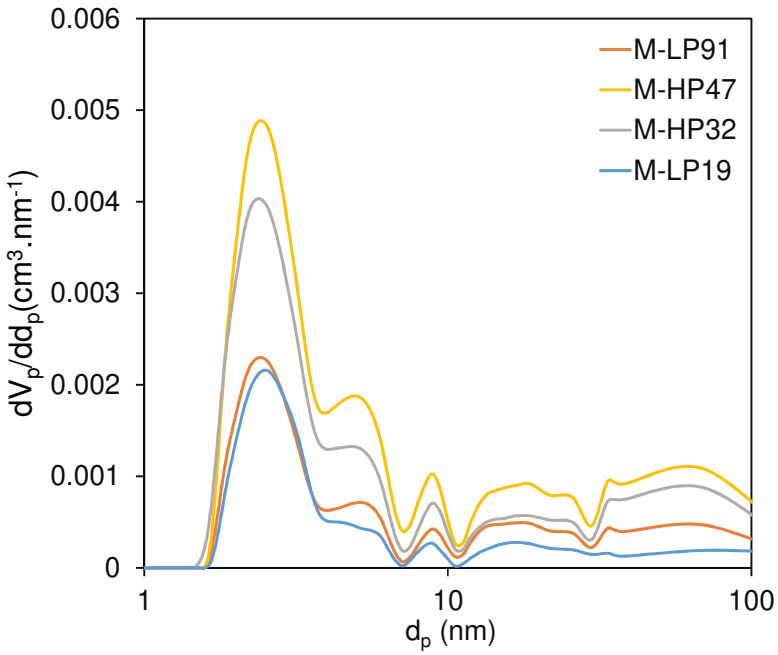

Figure 1: Pore size distribution of the Kynar® PVDF hollow fibre membranes based on N_2 adsorption isotherm

2.2.2. Particle suspension

Bentonite clay solution was prepared by dispersing 30 g of bentonite powder in 1 L of sodium azide solution (1 mg L^{-1} of NaN_3 in ultra-pure water to prevent from bacterial growth) under mechanical agitation for 15 hours. A stock solution of 18.1 g L^{-1} was obtained by successive decantation of the bentonite clay solution [39]. Feed solution with a bentonite particle concentration of 0.05 g L^{-1} was prepared from the stock solution (18.1 g L^{-1}). The ionic strength was adjusted to 10^{-3} mol L^{-1} by adding monovalent (KCl) or bivalent salt ($CaCl_2$) and the suspension was placed under mechanical agitation overnight. Potassium chloride and calcium chloride were added to bentonite suspensions to modify the interaction between the bentonite particles [40], and therefore change the cake properties during the filtration process [37].Two feed solutions were prepared and filtered: a bentonite (KCl) and a bentonite ($CaCl_2$) suspension.

The turbidity, particle size and zeta potential were measured for the prepared feed suspensions: bentonite (KCl) and bentonite ($CaCl_2$). The turbidity was measured using a HACH Turbidimeter, Model 2100N. Calibration curves were established to calibrate the

turbidity with the particle concentration in both bentonite suspensions. The bentonite particle size and zeta potential were determined using the instrument Malvern Zetasizer Nano ZS90. The bentonite particles have a plate-like shape. However, they were assimilated to spherical particles by the instrument for size measurement. The given averaged particle size was therefore not exact but used for comparison between the two feed suspensions. Analytical measurements of the bentonite feed suspensions are reported in Table 2.

Table 2: Characteristics of 0.05 g L^{-1} bentonite feed suspensions with ionic strength at 10^{-3} M adjusted with KCl or $CaCl_2$ at pH=7.

Feed	Turbidity (NTU)	Conductivity (mS/cm)	Average Particle size (nm)	Min/max Particle size (nm)	Zeta potential (mV)
Bentonite (KCl)	20.7 ± 0.1	0.494 ± 0.02	610 ± 349	196/1200	-16 ± 1
Bentonite ($CaCl_2$)	26.9 ± 0.1	0.085 ± 0.001	490 ± 240	189/586	-18 ± 1

2.3. Filtration

2.3.1. Bentonite suspension filtration

A single hollow fibre of 27 cm length was centred into a module of 30 cm length and 1.3 cm diameter, and potted at both ends into epoxy glue. Bentonite (KCl) or bentonite ($CaCl_2$) suspension was filtered in dead-end filtration in outside-in mode. A permeate volume of 60 L m^{-2} was filtered under constant pressure at 0.8 bar in order to obtain an identical fouling density of 3 g m^{-2} for each membrane. The cake thickness was measured by an optical device allowing 0.7 µm of resolution per pixel. An averaged cake thickness of 17 ± 3 µm was measured on each membrane external surface after filtration (see method in Supplementary Information S 1). Temperature, pressure and permeate mass were continuously recorded with ABB Model SM1000 recorder. Bentonite was fully retained by each membrane (i.e. rejection rates equal to 100%) and only cake deposition was observed during membrane fouling (no pore blocking).

2.3.2. Membrane and cake resistance

In ultrafiltration, the permeate flux can be modelled by the resistance-in-series model based on Darcy's law (Eq. 3). A flux decline is observed when fouling occurs during suspension filtration with the increase of the cake hydraulic resistance.

$$J = \frac{1}{Sext} * \frac{dV_p}{dt} = \frac{TMP}{\mu_s * (R_m + R_c)} \quad \text{Eq. 3}$$

with J the permeate flux (L m^{-2} h^{-1}), t the time (h), R_m the membrane hydraulic resistance in outside-in mode (m^2 L^{-1}) measured at specific TMP, μ_s the water viscosity (bar h) and R_c the cake hydraulic resistance (m^2 L^{-1})

The membrane hydraulic resistance (R_m) for each membrane was calculated from permeability measurements in outside-in mode with ultrapure water at specific pressure. The hydraulic resistance of bentonite cake was determined for each bentonite feed suspension. As identical cake resistances were found at the end of the filtration and between the different membranes, mean cake resistance was calculated for all membranes for bentonite (KCl) and for bentonite ($CaCl_2$).

2.4. Backwash

2.4.1. Procedure

Once the membrane was fouled, the flow of permeate was reversed to perform a backwash at constant pressure to remove the cake and recover the permeability. Backwash at fixed transmembrane pressure (BTMP) was chosen to study the influence of the membrane mechanical properties, as membrane deformation (pore and diameter) is function of the applied stress or pressure. A single backwash step was performed at different pressures from 0.2 to 1.5 bar. The fouling and then the backwash step was repeated on new hollow fibre membrane for each backwash pressure.

BTMP was applied for a duration of 60 seconds in which backwash waters were collected. Membrane was then rinsed with water at low flow (2 L h^{-1}) at an ionic strength adjusted to 10^{-3} mol L^{-1} with KCl or $CaCl_2$ (salt of the filtration) to eliminate the detached cake fragments still present in the module but leaving the remaining fouling on the membrane.

2.4.2. Backwash fluxes

As backwash pressure was kept constant, the backwash flux was increasing during the backwash step due to the gradual elimination of the cake, and was difficult to measure due to short time scale (~seconds) of the cake removal. Therefore, the following data and the reasoning is made for the beginning of backwashing before the cake hydraulic resistance changes due to the cake removal and not considering the possible cake compressibility. The backwash flux (J_{bw}) was calculated for each backwash pressure by Eq. 4 using the Darcy's law and was only valid for the fouled membrane before cake removal.

$$J_{bw} = Lp'_f * BTMP = \frac{BTMP}{\mu_s * (R'_m + R_c)} \quad \text{Eq. 4}$$

with J_{bw} the backwash flux through the fouled membrane (L m^{-2} h^{-1}), $Lp_f{}'$ the permeability of the fouled membrane (L m^{-2} h^{-1} bar^{-1}) in inside-out mode and R'_m the membrane hydraulic resistance in inside-out mode (m^2 L^{-1}) measured at specific BTMP. The cake hydraulic resistance was assumed constant in outside-in or inside-out mode; the possible cake compressibility was not, therefore, took into account. However, the membrane resistance was dependent on the mode and the pressure due to membrane deformation. The membrane hydraulic resistance (R'_m) for each membrane was calculated from permeability measurements in inside-out mode with ultrapure water at specific pressure.

2.4.3. Evaluation of backwash efficiency

Concentration of suspended particles was determined by turbidity measurement (as described in Supplementary Information S 2).The backwash efficiency was assessed by the percentage of cake removed during a single backwash and was calculated by the mass balance method [7], [22] described in Eq. 5. The cake removal (CR) was calculated from the mass of bentonite deposited on the membrane and recovered after backwash.

$$CR = \frac{m_{bw}}{m_d} \quad \text{Eq. 5}$$

with CR the amount of cake removed during the backwash and m_{bw} the mass of bentonite cake collected in the backwash waters (kg).

3. Results and discussion

3.1. Structure, mechanical and surface properties of hollow fibre membranes

Spun membranes had different dimensions with an outer diameter in the range of 840 to 1390 µm and a diameter ratio between 1.6 and 2 (Table 1). The SEM pictures of the membrane morphology are shown in Figure 2. The inner structure varied from one fibre to another: M-LP19 had a full macrovoid structure whereas M-HP32 had a sponge-like structure. Others were composed of both sponge-like structure and macrovoids.

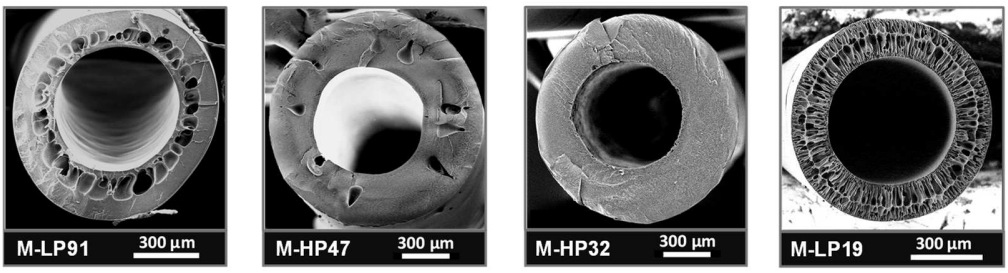

Figure 2: Cross-sectional SEM pictures of PVDF hollow fibre membranes.

Mechanical properties and especially Young's Modulus of membranes were purposely different to investigate the influence of the mechanical properties on the filtration and backwash process. Thus, the softest membrane M-LP19 had a Young's Modulus of 19 MPa while the most rigid membrane M-LP91 had a Young's Modulus of 91 MPa (Table 1). Stresses at break also reflected the weak mechanical properties of M-LP19 compared to M-LP91.

A water contact angle of about 50° was measured for the membranes M-LP91 and M-LP19 while a lower value of approximatively 40° was found for M-HP47 and M-HP32 meaning a more hydrophilic membrane surface (Table 1). The use of PVP in the preparation of M-HP47 and M-HP32 membranes was responsible for the increase in membrane hydrophilicity [41], [42].

3.2. Mass transfer properties

The membrane permeabilities measured in outside-in mode with ultra-pure water and at constant pressure, TMP=0.8 bar, are gathered in Table 1. M-LP19 and M-LP91 hollow fibre membranes had a low permeability (LP) in outside-in mode compared to M-HP32 and M-HP47, which had high permeability (HP). The presence of PVP in M-HP32 and M-HP47 greatly contributed to the increase in permeability [42].

However, as permeability is an intrinsic property of the membrane material, if it deforms under pressure the permeability becomes pressure dependent. Compaction of the pores is assumed to be responsible for a permeability loss of the membrane with increasing the pressure [43], [44] especially for elastic materials [45]. Due to various mechanical properties of the hollow fibres, the permeability behaviours of each membrane versus the pressure in outside-in and inside-out modes are plotted on Figure 3. The membrane permeability in outside-in mode was always below the permeability in inside-out mode suggesting a compaction effect due to external pressure. At a BTMP/TMP of 2.0 bar, the relative difference of the ultra-pure water permeability in inside-out mode ($Lp'_{2.0}$) to the permeability in outside-in mode ($Lp_{2.0}$) was 6%, 14%, 35% and 94% for M-LP91, M-HP47, M-HP32 and M-LP19 respectively. These results showed that a membrane with a low Young's Modulus was more sensitive to pressure and deformed to larger extent.

High recovery of the initial permeability was observed for M-LP91, M-HP47 and M-HP32 (reversibility from 97 to 100%) when the pressure was reduced from 2.4 to 0.2 bar. Regarding M-LP19, 95% of reversibility was measured when the pressure was reduced from 1.4 to 0.2 bar. However, the reversibility was lower (85%) when reducing the pressure from 2.4 to 0.2 bar, indicating a plastic deformation of the material. In inside-out mode, the permeability was constant when increasing the pressure for most membranes and was increasing for M-LP19. Enlargement of the pores was responsible for this increase in permeability for the softest fibre [34] as the pore density probably did not change.

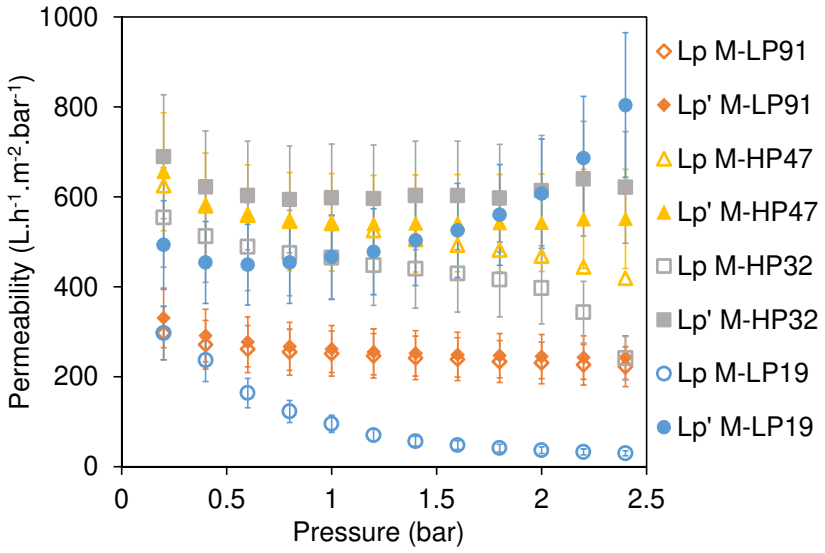

Figure 3: Pressure-dependence of membrane ultrapure water permeability in outside-in (Lp) and inside-out (Lp') modes.

3.3. Membrane fouling analysis

3.3.1. Bentonite cake resistance

Feed solutions were filtered to form a deposit of constant thickness on each hollow fibre membranes. The mean cake resistance was determined on all hollow fibre membranes and a common value was reported in Table 3 for each feed solutions.

Table 3: Mean cake resistance at the end of the filtration and before backwash.

Cake	R_c x10^{-11} (m^{-1})
Bentonite (KCl)	7.6 ± 0.5
Bentonite ($CaCl_2$)	1.9 ± 0.3

Low standard deviations were measured between the different hollow fibre membranes indicating similar hydraulic cake resistance and cake thickness for each fibre after filtration. The cake resistance of bentonite ($CaCl_2$) was 4 times lower than the resistance of bentonite (KCl) cake meaning that calcium chloride induced a more permeable bentonite cake structure than potassium chloride. In the presence of a monovalent and

inert salt, the interactions between particles were mainly repulsive leading to the formation of an ordered and low-permeable cake structure under pressure. Whereas in the case of a divalent salt, the interaction forces between particles were less repulsive and the distances between particles were not regular leading to a disordered and permeable cake structure under pressure [18].

3.3.2. Bentonite cake Young's modulus

Mechanical properties of wet filter cakes of bentonite (KCl) and bentonite ($CaCl_2$) were determined by indentation AFM measurements [46] at atmospheric pressure using mapping of force curves (i.e. ~ 1000 measurements over the surface area). The different suspensions of bentonite were filtered on a PVDF ultrafiltration flat-sheet membrane at constant pressure (TMP=0.8 bar) to form a 40 µm thick cake. Thick cake is needed to ensure the measurement of the Young's modulus of the cake and not the one of the membrane. Mean Young's modulus was calculated for bentonite (KCl) and bentonite ($CaCl_2$) cake and reported in Table 4.

Table 4: Mean Young's modulus for bentonite (KCl) and bentonite ($CaCl_2$) cake based on AFM measurements

Cake	**Mean Young's modulus** (MPa)
Bentonite (KCl)	0.004 ± 0.005
Bentonite ($CaCl_2$)	0.9 ± 0.9

Both cakes were mechanically non-homogenous with a large distribution of the Young's modulus other thousand measurement points. However, the order of magnitude of Young's modulus was very different: Bentonite (KCl) was much softer than bentonite ($CaCl_2$) with a mean Young's modulus 200 times lower.

3.4. Fouling removal analysis

3.4.1. Impact of the backwash pressure

Each fouled membrane was backwashed and the amount of cake removed was compared between the different hollow fibre membranes. Figure 4 shows increases of the percentage of bentonite (KCl) cake removal with increasing the backwash pressure for all membranes. A percentage of removal below 40% was observed in the case of M-LP91 and M-LP19 membranes at low BTMP [0.2-0.4 bar] whereas at BTMP=1.5 bar the removal percentage reached 70%. Low BTMP were however sufficient to remove the cake formed on M-HP32 and M-HP47 since 70% of the cake was removed at BTMP= 0.4 bar.

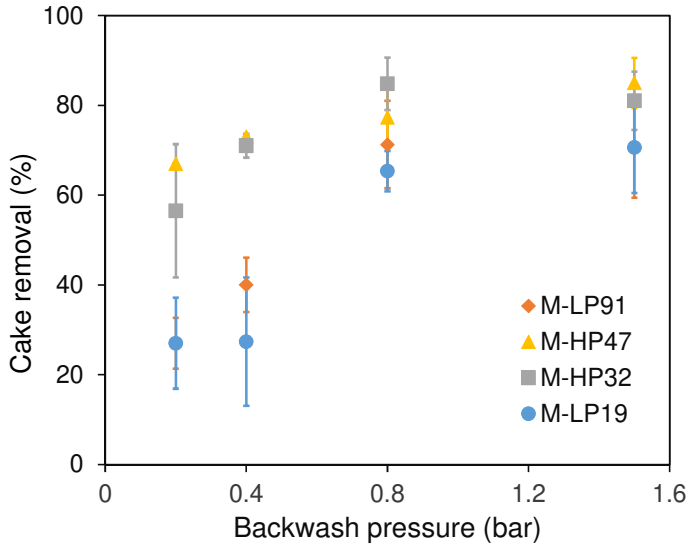

Figure 4: Effect of backwash pressure on bentonite (KCl) cake removal.

The experiments were reproduced in the exact same conditions but with bentonite ($CaCl_2$) feed solution. The amount of cake removed during the backwash step was also increasing with increasing the BTMP as observed on Figure 5. Contrary to the deposit with KCl, the deposit here was not removed at all at low BTMP, indeed less than 5% was removed at 0.2 bar for all fibres and less than 30% at 0.4 bar for most fibres (expect M-HP32). Furthermore, at high pressure the removal percentages were higher than in the case of cake made from bentonite (KCl). These results suggested a stronger cohesion of the cake. This was confirmed by visual observations of the cake fragmentation (Figure 6) and cake mechanical properties from AFM measurements (Table 4).

The cake with $CaCl_2$, which has a Young's modulus of 0.9 MPa, detached from the surface only as large pieces (several millimeters of typical size) at high pressure whereas the bentonite (KCl) cake, which has a Young's modulus of 0.004 MPa, was breaking into small pieces (several micrometer of typical size) at low and high pressures.

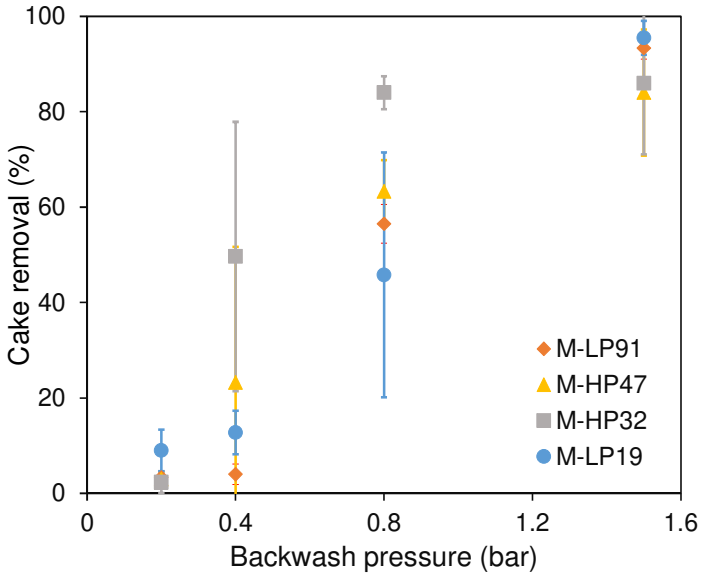

Figure 5: Effect of backwash pressure on bentonite ($CaCl_2$) cake removal.

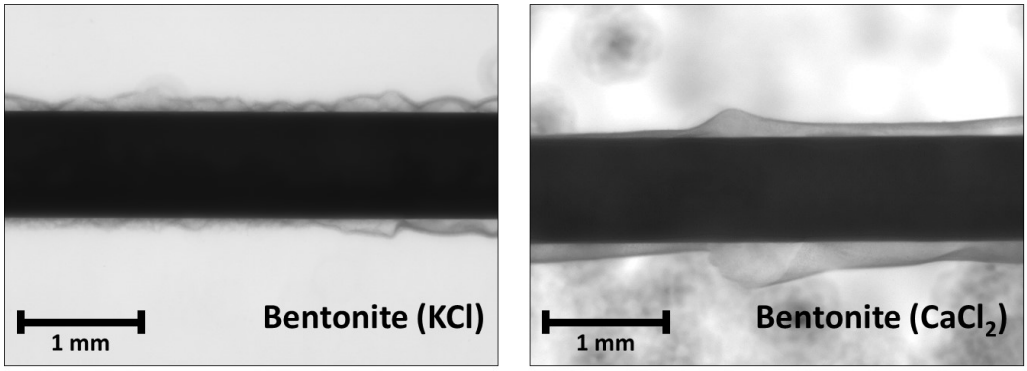

Figure 6: Pictures of bentonite (KCl) (left) and bentonite ($CaCl_2$) (right) cake fragments taken at the beginning of the backwash of MLP91 hollow fibre membrane (black central part of the picture) using an optical device (described in Supplementary Information S 1).

3.5. Critical backwash flux

High permeability membranes (see Table 1) demonstrated higher backwash efficiency as observed on Figure 4 and Figure 5. At same BTMP, the backwash flux was actually higher for M-HP32 and M-HP47 than for M-LP91 and M-LP19 and led to higher cake removal. Figure 7 and Figure 8 show the cake removal for both suspensions and the different fibres as a function of the backwash flux (J_{bw}). A generalized trend can be observed whatever the fibre but specific to the feed composition. The fouling removal mechanism seemed independent of the membrane composition and properties (membrane structure, dimensions, and mechanical, surface or mass transfer properties), only the operating backwash flux was causing here the elimination of the bentonite deposit.

Therefore, the bentonite cake removal using backwashing was controlled by the hydraulic vector and the cake properties as differences were observed between KCl and $CaCl_2$ bentonite suspension. However, the backwash flux was related to the permeability in inside-out which was linked to the pore size and pore density of the membrane.

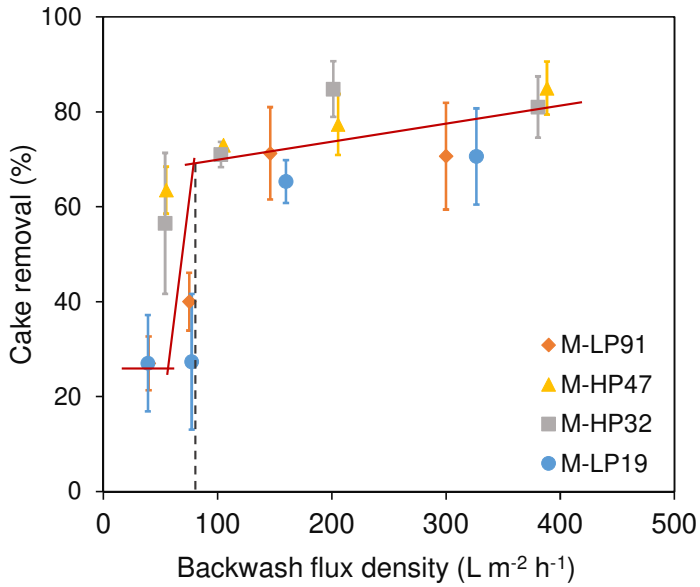

Figure 7: Effect of backwash flux on bentonite (KCl) cake removal. Red lines are only indicative curves.

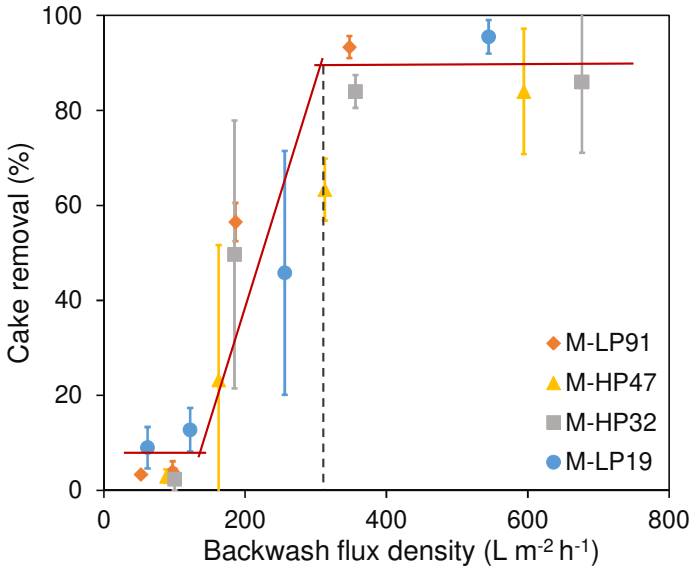

Figure 8: Effect of backwash flux on bentonite ($CaCl_2$) cake removal. Red lines are only indicative curves.

Three distinguished parts of the curve were identified from Figure 7 and Figure 8: a plateau at low J_{bw} where low removal occurred; a transition zone where the cake removal increased drastically and a plateau at high J_{bw} where significant amount of cake was removed but the increase of cake removal was low.

One can defined a critical backwash flux ($J_{bw,crit}$) as the minimal backwash flux to reach the plateau and from which the backwash reaches its maximal (or close to) efficiency.

In the case of bentonite (KCl) deposit, the critical backwash flux was 80 L m^{-2} h^{-1} whereas in the case of bentonite ($CaCl_2$) deposit, it was 310 L m^{-2} h^{-1}. The critical backwash flux was 4 times higher when the cake hydraulic resistance was 4 times lower (as seen on Table 3). This higher $J_{bw,crit}$ ($CaCl_2$) meant a cake that was more difficult to remove as shown previously in Figure 5. The critical backwash flux depended on the cake resistance, which was the result of filtration operating conditions (here, feed composition).

3.6. Inter cake-membrane pressure

The critical backwash flux is also closely related to a critical pressure required to detach and remove the bentonite cake. Indeed the applied backwash transmembrane pressure

generates a backwash flux, thus the critical backwash pressure ($BTMP_{crit}$) is also calculated from the critical backwash flux by Eq. 6.

$$BTMP_{crit} = \frac{J_{bw,crit}}{Lp'_f} \quad \text{Eq. 6}$$

However, BTMP was not the pressure that acted directly on the cake. We defined therefore the inter cake-membrane pressure (ICMP) as the pressure at the interface between the cake and the outer surface of the membrane. This pressure, or constraint, was indeed really applied on the cake surface. ICMP was obviously different from the backwash transmembrane pressure as the membrane offers hydraulic resistance to the water flux. ICMP was obtained from flow conservation for incompressible fluid and resistances in series model (Eq. 7, demonstration in Supplementary Information S 3) and calculated as:

$$ICMP = \frac{R_c}{R'_m + R_c} * BTMP \quad \text{Eq. 7}$$

with $ICMP$ the inter cake-membrane pressure (bar).

The inter cake-membrane pressure depends only on the cake and membrane hydraulic resistance and the backwash pressure. In this study, the hydraulic cake resistance was found constant for each fibre (see Table 3) for a given feed while the membrane resistance changes for each fibre.

The critical inter-cake membrane pressure $ICMP_{crit}$ can be calculated by Eq. 8:

$$ICMP_{crit} = \frac{R_c}{R'_m + R_c} * BTMP_{crit} \quad \text{Eq. 8}$$

By using Eq. 6 and Eq. 8, the critical backwash transmembrane pressure ($BTMP_{crit}$) and critical inter cake-membrane pressure ($ICMP_{crit}$) were calculated at the critical backwash flux. $BTMP_{crit}$ and $ICMP_{crit}$ for each membrane and feed solution are listed in Table 5.

Table 5: Critical backwash transmembrane pressures and critical inter cake-membrane pressure in the case of bentonite (KCl) and bentonite ($CaCl_2$) filtration.

Fibre	**Bentonite (KCl)**		**Bentonite ($CaCl_2$)**	
	$BTMP_{crit}$ (bar)	*$ICMP_{crit}$ (bar)*	*$BTMP_{crit}$ (bar)*	*$ICMP_{crit}$ (bar)*
M-LP19	0.41	0.17	0.85	0.16
M-HP32	0.30		0.70	
M-HP47	0.29		0.79	
M-LP91	0.43		1.34	

While large variations of $BTMP_{crit}$ were observed between fibres and the treated feed, $ICMP_{crit}$ was independent of the membrane and converged to a common value for both bentonite suspensions (with KCl or $CaCl_2$) as seen in Table 5. Indeed, the mean inter cake-membrane pressure at $BTMP_{crit}$ was equal to 0.17 bar. This $ICMP_{crit}$ reflected the pressure, as a mechanical constraint, needed for the detachment and removal of bentonite cakes, which was independent of the nature of the added salt as observed on Figure 9.

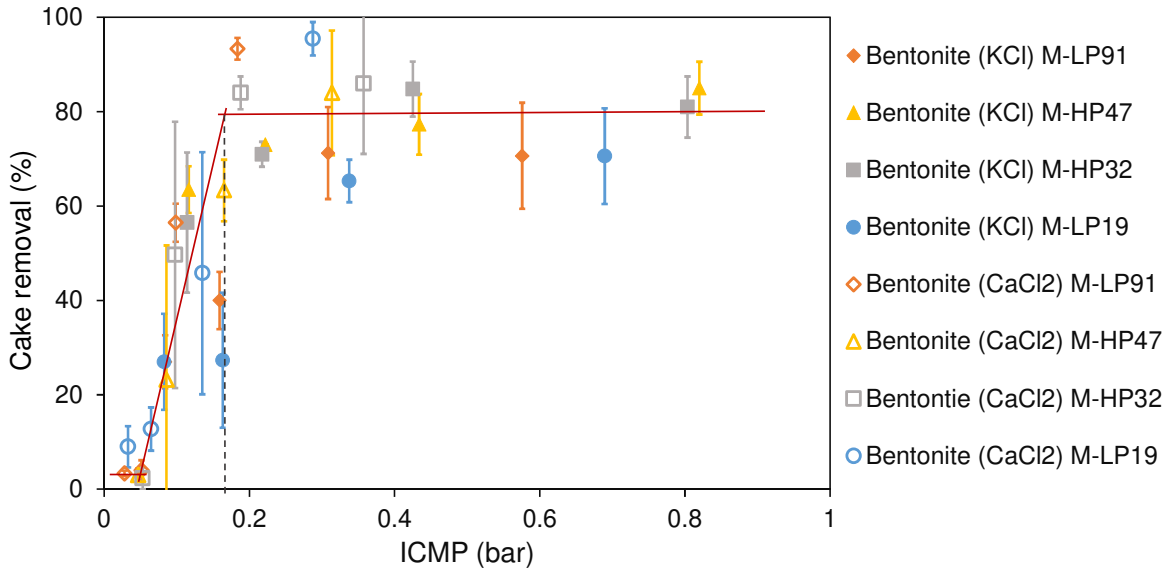

Figure 9: Effect of the inter cake-membrane pressure (ICMP) on the removal of bentonite cakes. Red lines are only indicative curves.

The same value of $ICMP_{crit}$ for two different cake hydraulic resistances indicates that the fouling removal mechanism was closely related to the ICMP. Bentonite (KCl) or bentonite ($CaCl_2$) cakes had different Young's moduli (see Table 4) which correspond to the observed fragmentation of the deposit (Figure 6): a low modulus leads to the fragmentation of the cake in small pieces whereas a high modulus leads to the large fragmented pieces of cake. However, despite very different Young's modulus, the same strength as pressure is needed to reach high cake removal efficiency (Figure 9). This suggests therefore that the cakes have the same adherence (or in the same order of) to the membrane despite different hydrophilicity of membrane surfaces (see Table 1). Estimation of the adhesion energy of bentonite cake to PVDF membrane is low and far below the energy spent hydraulically through the membrane during backwash [47]. These observations are in accordance with numerical study by Lohaus *et al.* [32] which shows particle to membrane interactions (i.e. adhesion) dominates the backwash efficiency over the particle to particle interactions (i.e. cake mechanical properties). They also show that decreasing the cake mechanical properties (for the same adhesion) leads to an increase of the backwash efficiency while remaining incomplete as in the case of bentonite (KCl) cake.

3.7. Discussion.

However, the critical inter cake-membrane pressure and the critical backwash flux are macroscopic values whereas the cake removal occurs at different scales from the particle to particle interaction and the particle to membrane interaction up to the membrane scale. On one hand, the three mechanisms described by Lohaus for one pore [32] (detachment of cluster of particles (i.e. aggregates), fragmentation of cluster and partial removal of particle aggregates from the pore structure) should occurred at the pore scale and be combined to the membrane pore size distributions. On the other hand, the pore size distribution should lead to a distribution of the ICMP (i.e. local ICMP) at the pore outlet (i.e. from the Poiseuille law, large pore has a lower hydraulic resistance than small pore) and to a distribution of backwash flux (i.e. local backwash flux). The fragmentation of the cake should be also related to the distribution of the cake Young's modulus as the standard deviations are large (see Table 4). Finally, one must keep in mind that the surface porosity of a membrane is in the range of 5 to 10% as commonly accepted: most of the cake is in contact of the membrane and could only be lifted at the pore outlets. A mechanically resistant cake is needed to be detached from the membrane as one large piece. At the opposite, a mechanically soft cake will be lifted and broken at the pore outlet reaming attached on the membrane surface without pore.

Figure 7, Figure 8 and Figure 9 clearly show three parts which could be described as:

i) At low flux, the cake removal efficiency is low: the ICMP is far lower the $ICMP_{crit}$ so the cake is not detached from the membrane nor fragmented. Detachment of weakly bounded particles or aggregates are removed. For bentonite (KCl), a better cake removal efficiency is obtained probably due to a low mechanical resistance or particle/to particle interactions compared to the bentonite ($CaCl_2$).

ii) A transition zone where the ICMP increases progressively with a local ICMP depending on the pore size: Large pores reach the $ICMP_{crit}$ before the smaller pores. At the pore outlet, the cake is lifted then fragmented in piece which size depends on the cake Young's modulus: Bentonite ($CaCl_2$) cake (with high Young's modulus) is efficiently removed as large piece showing high cake removal. Bentonite (KCl) cake (with low

Young's modulus) is fragmented in small pieces (i.e. over the pore outlet) and most of the cake remained attached to the membrane leading to low cake removal. Fragmentation of the cluster described by Lohaus occurs. The Young's modulus distributions of a cake should also lead to a partial fragmentation of the cake. The distributions of both flux and modulus are probably responsible for the large error bar observed in this part.

iii) At flux higher than the critical backwash flux or ICMP higher the $ICMP_{crit}$: the cake is lifted, fragmented as previously described and removed. The erosion of aggregates/pieces (i.e. removal of particle aggregates described by Lohaus) remaining attached at the membrane occurs. This induces a progressive increase of the cake removal efficiency for bentonite (KCl) which most of the cake remains on the membrane.

The $ICMP_{crit}$ is therefore a critical pressure required to lift and to eliminate the bentonite cake and appears independent of the membrane properties and the cake properties (see Table 5). $ICMP_{crit}$ is thus the needed force per square meter to overcome the adhesion forces which are obviously related to the surface properties of the membrane and the cake/membrane interactions. The $ICMP_{crit}$ is reached indirectly by applying a backwash transmembrane pressure, generating a flux through the membrane and the cake.Eq. 7 showed that membrane permeability (or membrane hydraulic resistance) is involved and membrane properties are therefore indirectly involved in the fouling removal. Therefore, a highly permeable membrane in inside-out mode would be a relevant candidate for bentonite ultrafiltration and good backwash efficiency. According to Darcy's law, the critical backwash flux, as the minimal backwash flux, can be determined by Eq. 9 by measuring the cake hydraulic resistance in the case of bentonite cake.

$$J_{bw,crit} = \frac{ICMP_{crit}}{R_c * \mu_s} \qquad \text{Eq. 9}$$

However, this scenario remains partially hypothetical and related to the studied cakes. In our case, all used membranes were PVDF ones and so the particle to membrane interactions or adhesion energies should be in the same range. Adherence to the membrane and mechanical properties of the cake were playing an important role so the measurement of the adhesion energy and cake mechanical properties are needed as well as the study of other cakes with high or low adhesion energies and high or low mechanical properties. The described mechanism is mechanically oriented and cakes are assumed rigid and isotropic (only the compressive Young's modulus is considered) whereas cake mechanical properties have an elastic or a viscoelastic part as in the case of polymer gels, as well as, cake mechanical properties could be anisotropic. Further investigation was needed to extend the concept of the ICMP to other fouling cake and have a better understanding of the fouling removal mechanism.

This also suggests that the new studies on backwash efficiency and performances of low fouling membranes should be conducted at the same ICMP in order to correctly evaluate and compare the efficiency between membranes as the hydraulic vector (here the backwash flux) is related to the membrane permeability.

Regarding the membrane mechanical properties, even if; in our case, deformable membranes have higher permeability in inside-out mode at high pressure (this is interesting to reach the $ICMP_{crit}$), the membrane compaction during filtration drastically reduced the permeate flux. Therefore, a non-deformable membrane might be preferable for the ultrafiltration of bentonite. In ultrafiltration, determining the critical backwash flux for a specific membrane/feed system can provide optimal backwash operating conditions and lead to energy savings. The extrapolation of the results from bentonite to other fouling materials, which may have different interactions with the membrane surface, is questionable. However, highly deformable membranes may still help to improve backwash efficiency in the case of more adhesive foulants and cakes as mentioned in the literature [35], [48], [49].

3.8. Economic impact

The critical backwash flux was the minimal backwash flux necessary to reach high backwash efficiency for a specific filtration unit. Using a backwash flux much higher than the critical backwash flux leads to a higher use of permeate water and a higher energy consumption with a low gain on the cake removal. The knowledge of the critical backwash flux is then a key parameter to optimize economically the backwash step.

As it is seen in Figure 10 , the backwash efficiency reaches a high stationary value when plotted as a function of the energy ($\frac{e_{bw}}{S_{ext}}$) and permeate volume ($\frac{V_{bw}}{S_{ext}}$) per surface area consumed during a backwash. For example, in the case of bentonite ($CaCl_2$) cake and for a single backwash of 60 seconds duration, the requirements of energy and water for optimal cake removal were 1000 J/m² and 6 L/m² respectively. This energy consumption during backwash was significant since it represents 20% of the energy consumption of the filtration step of bentonite suspension (details about consumed energy and permeate calculations are given in Supplementary Information S 4). A backwash flux that is twice as high would result in an extra 20 % of energy contribution to the energy consumed for the filtration.

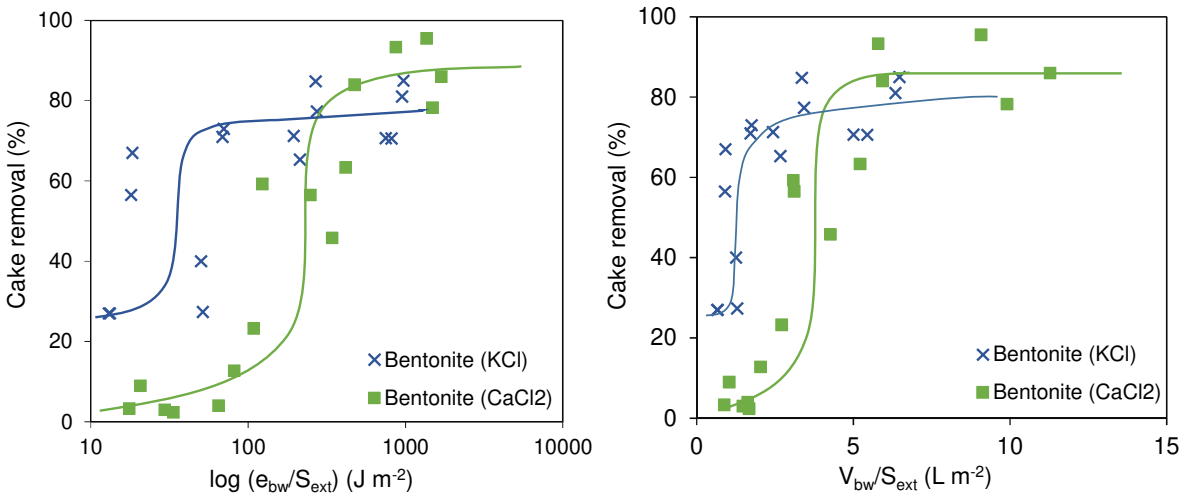

Figure 10: Backwash efficiency per consumed energy and permeate.

Energy consumption and net water production are therefore optimized if the membrane is cleaned at the critical backwash flux. Manufacturers could optimize the

filtration/backwash cycle by working at critical backwash flux determined from percentage of cake removal versus backwash flux curves for a specific feed system.

4. Conclusions

In summary, controlled dead-end ultrafiltration of bentonite suspension led to identical cake hydraulic resistances and cake thickness on 4 different Kynar® PVDF hollow fibre membranes (with different dimensions, mechanical, surface and mass transfer properties). Bentonite cake properties were dependent on the added salt and $CaCl_2$ strongly decreased the hydraulic resistance compared to KCl but induced a cake with a higher Young's modulus. Fouled membranes were backwashed and backwash efficiency was compared for these membranes. It has been found out that fouling removal mechanism in the case of bentonite filtration was mainly governed by the hydraulic vector that is the backwash flux and not by the intrinsic membrane properties. Indeed, the membrane deformation and membrane permeability seemed to not affect the mechanism of cake removal. We defined a critical backwash flux from which backwash reaches its highest efficiency and removes most of the deposit.
We defined the inter cake-membrane pressure which is the pressure between the cake and the membrane that occurs at the beginning of the backwash. The critical backwash flux corresponds to a critical inter cake-membrane pressure. The critical inter cake-membrane is the minimal pressure force (i.e. as strength) necessary to lift the cake before its fragmentation. It was found the same for all used PVDF membranes and formed bentonite cake indicating almost same adhesion energy. A mechanism for cake removal is finally proposed which involve three steps depending of the backwash flux and the ICMP.

5. Acknowledgements

This work was supported by Arkema S.A. (France) and the Chemical Engineering laboratory (Toulouse, France). We thank the ANRT for the CIFRE funding n° 2016/1131. We thank Dr Etienne Dague from the Systems Analysis and Architecture Laboratory (Toulouse, France) for AFM measurements.

6. References

[1] J. Davey, A.I. Schäfer, Ultrafiltration to supply safe drinking water in developing countries: A review of opportunities, in: Yanful E. (Ed.), Appropr. Technol. Environ. Prot. Dev. World, Springer science, 2009: pp. 151–168. https://doi.org/10.1007/978-1-4020-9139-1_16.

[2] H. Chang, H. Liang, F. Qu, B. Liu, H. Yu, X. Du, G. Li, S.A. Snyder, Hydraulic backwashing for low-pressure membranes in drinking water treatment: A review, J. Memb. Sci. 540 (2017) 362–380. https://doi.org/10.1016/j.memsci.2017.06.077.

[3] D. Jermann, W. Pronk, S. Meylan, M. Boller, Interplay of different NOM fouling mechanisms during ultrafiltration for drinking water production, Water Res. 41 (2007) 1713–1722. https://doi.org/10.1016/j.watres.2006.12.030.

[4] I.-S. Chang, P. Le Clech, B. Jefferson, S. Judd, Membrane Fouling in Membrane Bioreactors for Wastewater Treatment, J. Environ. Eng. 128 (2002) 1018–1029. https://doi.org/10.1061/(ASCE)0733-9372(2002)128:11(1018).

[5] Y. Miura, Y. Watanabe, S. Okabe, Membrane biofouling in pilot-scale membrane bioreactors (MBRs) treating municipal wastewater: Impact of biofilm formation, Environ. Sci. Technol. 41 (2007) 632–638. https://doi.org/10.1021/es0615371.

[6] Z. Geng, E.R. Hall, P.R. Bérubé, Membrane fouling mechanisms of a membrane enhanced biological phosphorus removal process, J. Memb. Sci. 296 (2007) 93–101. https://doi.org/10.1016/j.memsci.2007.03.019.

[7] P.J. Remize, C. Guigui, C. Cabassud, Evaluation of backwash efficiency, definition of remaining fouling and characterisation of its contribution in irreversible fouling: Case of drinking water production by air-assisted ultra-filtration, J. Memb. Sci. 355 (2010) 104–111. https://doi.org/10.1016/j.memsci.2010.03.005.

[8] V. Puspitasari, A. Granville, P. Le-Clech, V. Chen, Cleaning and ageing effect of sodium hypochlorite on polyvinylidene fluoride (PVDF) membrane, Sep. Purif. Technol. 72 (2010) 301–308. https://doi.org/10.1016/j.seppur.2010.03.001.

[9] L. Vanysacker, R. Bernshtein, I.F.J. Vankelecom, Effect of chemical cleaning and membrane aging on membrane biofouling using model organisms with increasing complexity, J. Memb. Sci. 457 (2014) 19–28.

https://doi.org/10.1016/j.memsci.2014.01.015.

[10] B. Pellegrin, F. Mezzari, Y. Hanafi, A. Szymczyk, J.C. Remigy, C. Causserand, Filtration performance and pore size distribution of hypochlorite aged PES/PVP ultrafiltration membranes, J. Memb. Sci. 474 (2015) 175–186. https://doi.org/10.1016/j.memsci.2014.09.028.

[11] O. Ferrer, B. Lefèvre, G. Prats, X. Bernat, O. Gibert, M. Paraira, Reversibility of fouling on ultrafiltration membrane by backwashing and chemical cleaning: differences in organic fractions behaviour, Desalin. Water Treat. 57 (2016) 8593–8607. https://doi.org/10.1080/19443994.2015.1022807.

[12] F. Meng, S. Zhang, Y. Oh, Z. Zhou, H.S. Shin, S.R. Chae, Fouling in membrane bioreactors: An updated review, Water Res. 114 (2017) 151–180. https://doi.org/10.1016/j.watres.2017.02.006.

[13] W. Gao, H. Liang, J. Ma, M. Han, Z. lin Chen, Z. shuang Han, G. bai Li, Membrane fouling control in ultrafiltration technology for drinking water production: A review, Desalination. 272 (2011) 1–8. https://doi.org/10.1016/j.desal.2011.01.051.

[14] X. Shi, G. Tal, N.P. Hankins, V. Gitis, Fouling and cleaning of ultrafiltration membranes: A review, J. Water Process Eng. 1 (2014) 121–138. https://doi.org/10.1016/j.jwpe.2014.04.003.

[15] N. Hilal, O.O. Ogunbiyi, N.J. Miles, R. Nigmatullin, Methods employed for control of fouling in MF and UF membranes: A comprehensive review, Sep. Sci. Technol. 40 (2005) 1957–2005. https://doi.org/10.1081/SS-200068409.

[16] P. Bacchin, P. Aimar, Critical fouling conditions induced by colloidal surface interaction: From causes to consequences, Desalination. 175 (2005) 21–27. https://doi.org/10.1016/j.desal.2004.09.020.

[17] P. Bacchin, B. Espinasse, P. Aimar, Distributions of critical flux: Modelling, experimental analysis and consequences for cross-flow membrane filtration, J. Memb. Sci. 250 (2005) 223–234. https://doi.org/10.1016/j.memsci.2004.10.033.

[18] Vincent Lelievre, Rhéologie et filtration de dispersions aqueuses de nanoparticules d'hectorite en relation avec la structuration des dépôts, PhD Dissertation, University of Grenoble INPG, 2005.

[19] C. Martin, F. Pignon, A. Magnin, M. Meireles, V. Lelièvre, P. Lindner, B. Cabane, Osmotic compression and expansion of highly ordered clay dispersions, Langmuir. 22 (2006) 4065–4075. https://doi.org/10.1021/la052605k.

[20] F. Pignon, A. Magnin, J.M. Piau, B. Cabane, P. Lindner, O. Diat, Yield stress thixotropic clay suspension: Investigations of structure by light, neutron, and x-ray scattering, Phys. Rev. E - Stat. Physics, Plasmas, Fluids, Relat. Interdiscip. Top. 56 (1997) 3281–3289. https://doi.org/10.1103/PhysRevE.56.3281.

[21] A. Mourchid, A. Delville, J. Lambard, E. Lécolier, P. Levitz, Phase Diagram of Colloidal Dispersions of Anisotropic Charged Particles: Equilibrium Properties, Structure, and Rheology of Laponite Suspensions, Langmuir. 11 (1995) 1942–1950. https://doi.org/10.1021/la00006a020.

[22] C. Serra, L. Durand-Bourlier, M.J. Clifton, P. Moulin, J.C. Rouch, P. Aptel, Use of air sparging to improve backwash efficiency in hollow-fiber modules, J. Memb. Sci. 161 (1999) 95–113. https://doi.org/10.1016/S0376-7388(99)00106-4.

[23] C. Cabassud, S. Laborie, L. Durand-Bourlier, J.M. Lainé, Air sparging in ultrafiltration hollow fibers: Relationship between flux enhancement, cake characteristics and hydrodynamic parameters, J. Memb. Sci. 181 (2001) 57–69. https://doi.org/10.1016/S0376-7388(00)00538-X.

[24] C. Psoch, S. Schiewer, Anti-fouling application of air sparging and backflushing for MBR, J. Memb. Sci. 283 (2006) 273–280. https://doi.org/10.1016/j.memsci.2006.06.042.

[25] L. Li, H.E. Wray, R.C. Andrews, P.R. Bérubé, Ultrafiltration Fouling: Impact of Backwash Frequency and Air Sparging, Sep. Sci. Technol. 49 (2014) 2814–2823. https://doi.org/10.1080/01496395.2014.948964.

[26] Y. Ye, V. Chen, P. Le-Clech, Evolution of fouling deposition and removal on hollow fibre membrane during filtration with periodical backwash, Desalination. 283 (2011) 198–205. https://doi.org/10.1016/j.desal.2011.03.087.

[27] E.H. Bouhabila, R. Ben Aïm, H. Buisson, Fouling characterisation in membrane bioreactors, Sep. Purif. Technol. 22–23 (2001) 123–132. https://doi.org/10.1016/S1383-5866(00)00156-8.

[28] C. Albasi, Y. Bessiere, S. Desclaux, J.C. Remigy, Filtration of biological sludge by

immersed hollow-fiber membranes: Influence of initial permeability choice of operating conditions, Desalination. 146 (2002) 427–431. https://doi.org/10.1016/S0011-9164(02)00527-1.

[29] P.J. Smith, S. Vigneswaran, H.H. Ngo, R. Ben-Aim, H. Nguyen, A new approach to backwash initiation in membrane systems, J. Memb. Sci. 278 (2006) 381–389. https://doi.org/10.1016/j.memsci.2005.11.024.

[30] H. Huang, N. Lee, T. Young, A. Gary, J.C. Lozier, J.G. Jacangelo, Natural organic matter fouling of low-pressure, hollow-fibre membranes: Effects of NOM source and hydrodynamic conditions, Water Res. 41 (2007) 3823–3832. https://doi.org/10.1016/j.watres.2007.05.036.

[31] K.J. Hwang, C.S. Chan, K.L. Tung, Effect of backwash on the performance of submerged membrane filtration, J. Memb. Sci. 330 (2009) 349–356. https://doi.org/10.1016/j.memsci.2009.01.012.

[32] J. Lohaus, F. Stockmeier, P. Surray, J. Lölsberg, M. Wessling, What are the microscopic events during membrane backwashing? J. Memb. Sci. 602 (2020). https://doi.org/10.1016/j.memsci.2020.117886.

[33] H. Chang, F. Qu, B. Liu, H. Yu, K. Li, S. Shao, G. Li, H. Liang, Hydraulic irreversibility of ultrafiltration membrane fouling by humic acid: Effects of membrane properties and backwash water composition, J. Memb. Sci. 493 (2015) 723–733. https://doi.org/10.1016/j.memsci.2015.07.001.

[34] E. Akhondi, F. Zamani, A.W.K. Law, W.B. Krantz, A.G. Fane, J.W. Chew, Influence of backwashing on the pore size of hollow fibre ultrafiltration membranes, J. Memb. Sci. 521 (2017) 33–42. https://doi.org/10.1016/j.memsci.2016.08.070.

[35] V. Levering, Q. Wang, P. Shivapooja, X. Zhao, G.P. López, Soft robotic concepts in catheter design: An on-demand fouling-release urinary catheter, Adv. Healthc. Mater. 3 (2014) 1588–1596. https://doi.org/10.1002/adhm.201400035.

[36] N. Kalboussi, J. Harmand, A. Rapaport, T. Bayen, F. Ellouze, N. Ben Amar, Optimal control of physical backwash strategy - towards the enhancement of membrane filtration process performance, J. Memb. Sci. 545 (2018) 38–48. https://doi.org/10.1016/j.memsci.2017.09.053.

[37] S.R. Santiwong, J. Guan, T.D. Waite, Effect of ionic strength and pH on hydraulic properties and structure of accumulating solid assemblages during microfiltration of montmorillonite suspensions, J. Colloid Interface Sci. 317 (2008) 214–227. https://doi.org/10.1016/j.jcis.2007.09.052.

[38] H. Shi, L. Xue, A. Gao, Y. Fu, Q. Zhou, L. Zhu, Fouling-resistant and adhesion-resistant surface modification of dual layer PVDF hollow fiber membrane by dopamine and quaternary polyethyleneimine, J. Memb. Sci. 498 (2016) 39–47. https://doi.org/10.1016/j.memsci.2015.09.065.

[39] Y. Bessiere, Filtration Frontale sur membrane : mise en evidence du volume filtre critique pour l'anticipation et le controle du colmatage, PhD Dissertation, University of Toulouse Paul Sabatier, 2005.

[40] D. Niriella, R.P. Carnahan, Comparison study of zeta potential values of bentonite in salt solutions, J. Dispers. Sci. Technol. 27 (2006) 123–131. https://doi.org/10.1081/DIS-200066860.

[41] E. Fontananova, M.A. Bahattab, S.A. Aljlil, M. Alowairdy, G. Rinaldi, D. Vuono, J.B. Nagy, E. Drioli, G. Di Profio, From hydrophobic to hydrophilic polyvinylidenefluoride (PVDF) membranes by gaining new insight into material's properties, RSC Adv. 5 (2015) 56219–56231. https://doi.org/10.1039/c5ra08388e.

[42] Y.W. Guo, W.W. Cui, W.H. Xu, Y. Jiang, H.H. Liu, J.Y. Xu, Z.Q. Gao, L.Z. Liu, Effect of PVP hydrophilic additive on the morphology and properties of PVDF porous membranes, Adv. Mater. Res. 981 (2014) 891–894. https://doi.org/10.4028/www.scientific.net/AMR.981.891.

[43] S. Stade, M. Kallioinen, A. Mikkola, T. Tuuva, M. Mänttäri, Reversible and irreversible compaction of ultrafiltration membranes, Sep. Purif. Technol. 118 (2013) 127–134. https://doi.org/10.1016/j.seppur.2013.06.039.

[44] K.M. Persson, V. Gekas, G. Trägårdh, Study of membrane compaction and its influence on ultrafiltration water permeability, J. Memb. Sci. 100 (1995) 155–162. https://doi.org/10.1016/0376-7388(94)00263-X.

[45] J. Sierke, A. V. Ellis, Cross-linking of dehydrofluorinated PVDF membranes with thiol modified polyhedral oligomeric silsesquioxane (POSS) and pure water flux analysis, J. Memb. Sci. 581 (2019) 362–372.

https://doi.org/10.1016/j.memsci.2019.03.063.

[46] H.J. Butt, B. Cappella, M. Kappl, Force measurements with the atomic force microscope: Technique, interpretation and applications, Surf. Sci. Rep. 59 (2005) 1–152. https://doi.org/https://doi.org/10.1016/j.surfrep.2005.08.003.

[47] T. Vroman, Mécanismes de décolmatage de membranes fibres creuses en traitement des eaux: Flux critique de rétrolavage et déformation de la membrane pour une amélioration de l'efficacité du rétrolavage, PhD Dissertation, University of Toulouse Paul Sabatier, 2020.

[48] P. Shivapooja, Q. Wang, L.M. Szott, B. Orihuela, D. Rittschof, X. Zhao, G.P. López, Dynamic surface deformation of silicone elastomers for management of marine biofouling: laboratory and field studies using pneumatic actuation, Biofouling. 31 (2015) 265–274. https://doi.org/10.1080/08927014.2015.1035651.

[49] G. Limbert, R. Bryan, R. Cotton, P. Young, L. Hall-Stoodley, S. Kathju, P. Stoodley, On the mechanics of bacterial biofilms on non-dissolvable surgical sutures: A laser scanning confocal microscopy-based finite element study, Acta Biomater. 9 (2013) 6641–6652. https://doi.org/10.1016/j.actbio.2013.01.017.

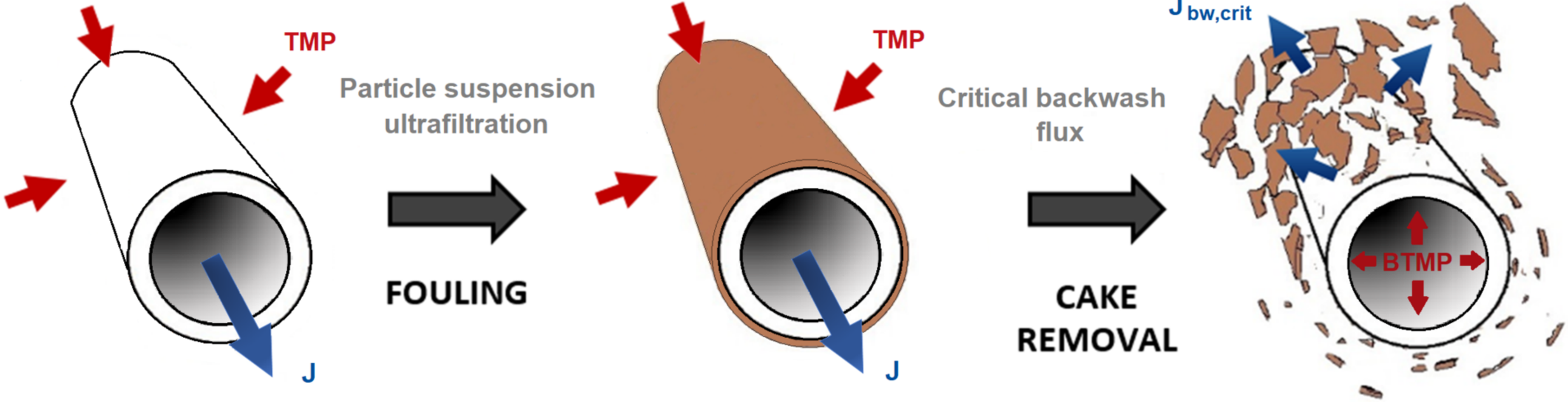
TMP
J
Particle suspension
ultrafiltration
FOULING
TMP
J
Critical backwash
flux
CAKE
REMOVAL
J bw,crit
BTMP